The Astrophysical Journal Letters, 741:L8 (6pp), 2011 November 1 doi:10.1088/2041-8205/741/1/L8

ON THE MASS-LOSS RATE OF MASSIVE STARS IN THE LOW-METALLICITY GALAXIES IC 1613, WLM, AND NGC 3109*

F. Tramper, H. Sana, A. de Koter, and L. Kaper
Astronomical Institute "Anton Pannekoek," University of Amsterdam, Science Park 904, 1098 XH Amsterdam, The Netherlands; F.Tramper@uva.nl
Received 2011 September 6; accepted 2011 September 22; published 2011 October 7

ABSTRACT

We present a spectroscopic analysis of Very Large Telescope/X-Shooter observations of six O-type stars in the low-metallicity ($Z \sim 1/7\ Z_\odot$) galaxies IC 1613, WLM, and NGC 3109. The stellar and wind parameters of these sources allow us, for the first time, to probe the mass loss versus metallicity dependence of stellar winds at metallicities below that of the Small Magellanic Cloud (at $Z \sim 1/5\ Z_\odot$) by means of a modified wind momentum versus luminosity diagram. The wind strengths that we obtain for the objects in WLM and NGC 3109 are unexpectedly high and do not agree with theoretical predictions. The objects in IC 1613 tend toward a higher than expected mass-loss rate, but remain consistent with predictions within their error bars. We discuss potential systematic uncertainties in the mass-loss determinations to explain our results. However, if further scrutinization of these findings point towards an intrinsic cause for this unexpected sub-SMC mass-loss behavior, implications would include a higher than anticipated number of Wolf–Rayet stars and Ib/Ic supernovae in low-metallicity environments, but a reduced number of long-duration gamma-ray bursts produced through a single-star evolutionary channel.

Key words: galaxies: individual (IC1613, WLM, NGC3109) – stars: massive – stars: mass-loss – stars: winds, outflows – techniques: spectroscopic

Online-only material: color figures

1. INTRODUCTION

The evolution of massive stars is greatly affected by the amount of mass and angular momentum lost during their lifetime. Understanding the mechanisms responsible for these losses is a fundamental goal in stellar astrophysics. For instance, mass loss influences the characteristics of the supernova explosion with which a massive star ends its life, as well as the number of potential single-star progenitors of long-duration gamma-ray bursts (e.g., Yoon & Langer 2005; Woosley & Bloom 2006).

An important mass-loss mechanism, at least at galactic and Magellanic Cloud metallicities, is the transfer of momentum from photons to the atmospheric gas through line interactions, initiating and driving an outflow (e.g., Castor et al. 1975; Kudritzki & Puls 2000; Vink et al. 2001). The strength of these radiation-driven winds therefore depends on the effective number of absorption lines, in particular near the photospheric flux maximum in the ultraviolet. It is dominated by the absorption of light through a copious amount of metallic ion lines that are present in this wavelength region. As a consequence, the mass-loss rate ($\dot{M}$) of stars hotter than 25,000 K is predicted to scale with metallicity (Z) as $\dot{M} \propto Z^{0.69\pm0.10}$ (Vink et al. 2001). Mokiem et al. (2007) showed that this prediction holds for early-type stars in the Galaxy ($Z = Z_\odot$), Large Magellanic Cloud (LMC; $Z = 0.5\ Z_\odot$), and Small Magellanic Cloud (SMC; $Z = 0.2\ Z_\odot$), yielding the empirical relation $\dot{M} \propto Z^{0.78\pm0.17}$. To date, however, no observational constraints exist at sub-SMC metallicities.

For galactic stars more luminous than $10^{5.8}\ L_\odot$ (i.e., above the Humphreys–Davidson limit), episodic mass loss is expected to occur during the luminous blue variable and/or Wolf–Rayet phase (e.g., Humphreys & Davidson 1994; Smith et al. 2004). Also, dust/pulsation-driven mass loss takes place in the red supergiant phase of lower luminosity objects (e.g., Heger et al. 1997; Yoon & Cantiello 2010). However, if the *relative* contribution of line driving remains sizable at all Z, an important consequence of the theory of radiation-driven winds would be that low-metallicity massive stars lose less mass and angular momentum over their lifetime than their high-metallicity counterparts. At sub-SMC metallicities, single stars with a large initial rotational velocity may avoid envelope expansion and the associated efficient transfer of angular momentum from the core to the envelope, thus keeping a rapidly spinning core. This makes them potential progenitors of long-duration gamma-ray bursts (e.g., Woosley & Bloom 2006).

In order to observationally constrain stellar and wind parameters at sub-SMC metallicities, we have used the X-Shooter spectrograph mounted on ESO's Very Large Telescope (VLT) UT2 (D'Odorico et al. 2006; Vernet et al. 2011) to secure intermediate-resolution spectra of some of the most massive stars in three nearby dwarf galaxies, IC 1613, WLM, and NCG 3109, each having a metallicity of $Z \approx 1/7\ Z_\odot$. The throughput of the instrument, combined with the collecting area of an 8.2 m telescope, allows us, for the first time, to perform a detailed quantitative spectral analysis at a resolution $R \sim 6000$–9000 and test the theory of line driving in O-type stars at a sub-SMC metallicity (see also Herrero et al. 2011).

With the aid of previous, low-resolution studies (Bresolin et al. 2006, 2007; Evans et al. 2007), we selected the six visually brightest O-type stars in these galaxies (four in IC 1613, one each in WLM and NGC 3109). The low line-of-sight extinction toward these galaxies and their similar metallicity allow us, for this particular study, to treat these stars as a group.

In Section 2, the observations and data reduction are described. Section 3 discusses the method of analysis and Section 4 presents the results. Finally, in Section 5, we discuss the implications of our findings.

* Based on VLT/X-Shooter observations under program 085D.0741.

Table 1
Properties of the Observed Stars

ID	R.A. (J2000)	Decl. (J2000)	V	M_V	Spectral Type	RV (km s^{-1})	12+log(O/H)
IC 1613							
–A13	01 05 06.21	+02 10 44.8	19.02	−5.55	O3 V((f))	−240	8.0
–A15	01 05 08.74	+02 10 01.1	19.35	−5.11	O9.5 III	−240	···
–B11	01 04 43.82	+02 06 46.1	18.68	−5.84	O9.5 I	−240	···
–C9	01 04 38.63	+02 09 44.4	19.02	−5.44	O8 III((f))	−265	···
WLM							
–A11	00 01 59.97	−15 28 19.2	18.40	−6.35	O9.7 Ia	−135	···
NGC 3109							
–20	10 03 03.22	−26 09 21.4	19.33	−6.67	O8 I	407	7.8

References. V-band magnitudes from Bresolin et al. (2007, IC1613), Bresolin et al. (2006, WLM), and Evans et al. (2007, NGC3109).

2. OBSERVATIONS AND DATA REDUCTION

The spectrum of NGC 3109-20 has been obtained during a X-Shooter Guaranteed Time Observations (GTO) run on 2010 April 23, with an exposure time of 5×900 s. In a successive GTO run from 2010 September 12 to 16, the stars in IC 1613 and WLM were observed, with an exposure time of 6×900 s for all stars. All observations were obtained in nodding mode with a nod throw of 5″, using a slit width of 0.″8 for the UVB arm (300–550 nm), 0.″9 for the VIS arm (550–1020 nm), and 0.″9 for the NIR arm (1000–2500 nm), yielding a spectral resolving power of R = 6200, 8800, and 5600, respectively. Conditions were clear or photometric with an average seeing below 0.″8 in the R band. The moon illumination fraction was below 0.2. Fundamental properties of the observed stars are listed in Table 1.

2.1. Data Reduction

The data have been reduced using the X-Shooter pipeline v1.2.2 in physical model mode (Goldoni et al. 2006; Modigliani et al. 2010). The nodding mode usually allows for easy nebular subtraction. However, all observations except those of WLM-A11 show signs of variable strength of the nebular emission lines over the length of the nod throw, preventing the use of this method. For these stars the sky subtraction was done by using suitable regions of sky close to the object, resulting in a good nebular correction for all stars except IC 1613-A15 (see below). The signal-to-noise ratio (S/N) per resolution element ranges from 32 to 67 in the UVB arm and from 21 to 29 in the VIS arm. The detected flux in the NIR part of the spectrum was low (S/N < 5), so we could not use this part of the spectrum in our analysis.

The nebular emission in IC 1613-A15 varies in radial velocity (RV) along the slit, causing residuals in the final spectrum. The regions affected by these residuals were removed from the final spectrum and not used in the atmosphere fit.

The resulting one-dimensional spectra were normalized to the continuum. Figure 1 presents the blue spectrum and Hα region of all six stars. Figure 2 shows the profiles of the mass-loss sensitive He II 4686 and Hα lines in more detail. The spectral type of the stars was determined by comparing with a spectral atlas of O-type stars (H. Sana et al. 2011, in preparation), and for all but one agree with the type listed in the literature. The only change is that the spectral type of IC1613-A13 is refined from O3-4 V((f)) (Bresolin et al. 2007) to O3 V((f)).

2.2. Oxygen Abundance Determination

In order to also provide an independent oxygen abundance measurement, a relative flux calibration was performed for the frames where nebular oxygen emission is present (IC 1613-A13 and NGC 3109-20), using spectra of photometric standard stars taken during each night of observations. To derive the oxygen abundance, we use the strong line method (Pagel et al. 1979) with the updated calibration by Pilyugin & Thuan (2005), using the [O II] λλ 3727,3729, [O III] λλ 4959,5007, and Hβ nebular emission lines. The resulting abundances are given in Table 1, and although abundances derived with the strong line method can have uncertainties up to 0.8 dex (see, e.g., Bresolin et al. 2009), our measures agree well with the literature values of 12 + log(O/H) = 7.90 ± 0.08 (IC 1613; Bresolin et al. 2007), 7.80 ± 0.07 (WLM; Urbaneja et al. 2008), and 7.76 ± 0.07 (NGC 3109; Evans et al. 2007) derived from B- and A-type supergiants.

3. MODELING

The stellar properties and wind characteristics of the stars have been determined using an automated fitting method developed by Mokiem et al. (2005). This method combines the non-LTE stellar atmosphere model FASTWIND (Puls et al. 2005) with the generic fitting algorithm PIKAIA (Charbonneau 1995). It allows for a fast and homogeneous analysis of our sample of stars using a selection of hydrogen, He I, and He II lines.

The absolute visual magnitude (M_V) of the stars is needed as an input parameter. They have been determined using the V magnitudes from Table 1 and a distance and reddening of d = 721 kpc (Pietrzyński et al. 2006) and $E(B-V)$ = 0.025 (Schlegel et al. 1998) for IC 1613, d = 995 kpc and $E(B-V)$ = 0.08 for WLM (Urbaneja et al. 2008), and d = 1300 kpc (Soszyński et al. 2006) and $E(B-V)$ = 0.14 (Davidge 1993) for NGC 3109. The resulting values of M_V agree well with the values for their spectral type (Martins et al. 2005). The RV has been measured by fitting a Gaussian profile to the hydrogen lines and the obtained values are in agreement with the radial velocities of the host galaxies.

The fitting algorithm covers a large parameter space, fitting line profiles of the same 11 spectral lines as described by Mokiem et al. (2005) to determine the effective temperature ($T_{\rm eff}$), surface gravity (g), mass-loss rate ($\dot{M}$), surface helium abundance ($Y_{\rm He}$), depth-independent microturbulent velocity ($v_{\rm tur}$), and projected rotational velocity ($v_{\rm rot}\sin i$). The bolometric luminosity L is derived by applying the bolometric correction to the absolute visual magnitude used as input. This luminosity, together with the obtained temperature, is then used to determine the radius (R) of the star. The terminal wind velocity (v_∞) cannot be constrained from the optical, but is related to the surface escape velocity $v_{\rm esc}$: $v_\infty = 2.6\ v_{\rm esc}$ (at $Z = Z_\odot$; Lamers

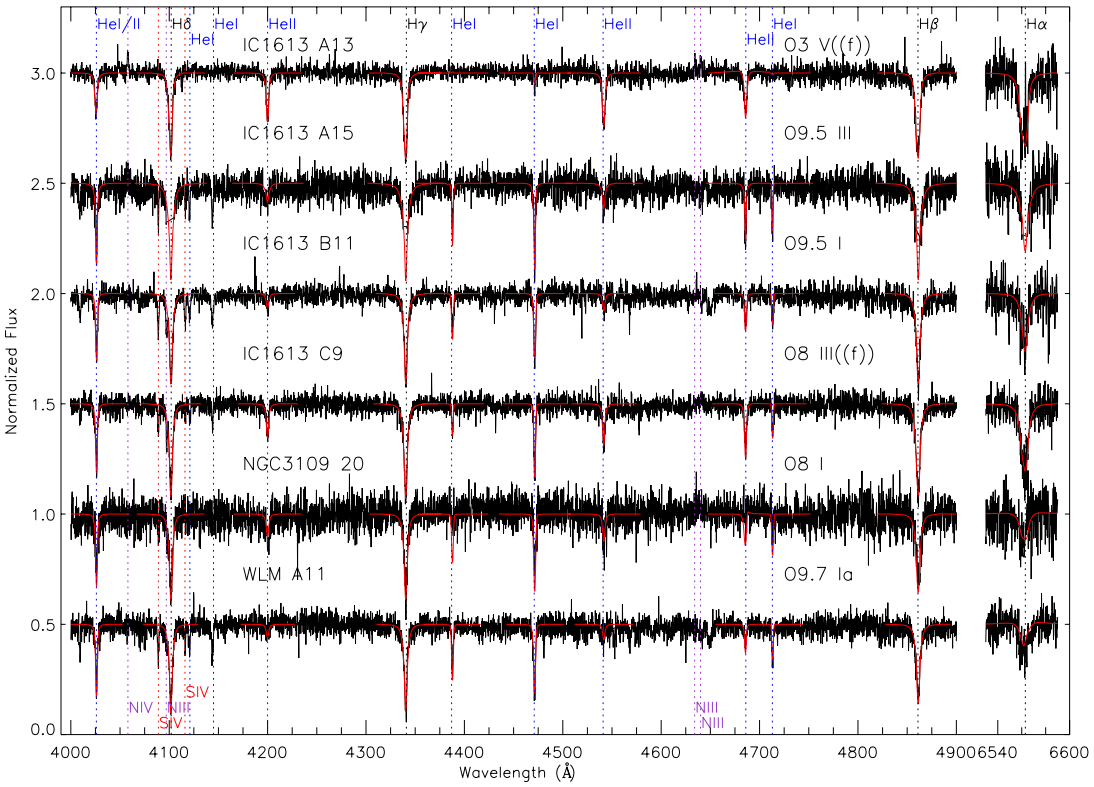

Figure 1. Selected regions of the normalized X-Shooter spectra of the observed O-stars. Overplotted in red are the best-fit line profiles for the fitted lines.

et al. 1995; Kudritzki & Puls 2000). The coefficient of the wind velocity structure β has been fixed to 0.8 for the dwarfs, 0.9 for the giants, and 0.95 for the supergiants, conforming with theoretical predictions (L. Muijres et al. 2011, in preparation).

Table 2 presents the best-fit values and derived properties for the six stars. The values for $T_{\rm eff}$ are higher than those of their Galactic counterparts of the same spectral type (Martins et al. 2005), in agreement with their low metallicity (Mokiem et al. 2004). IC 1613-A13 shows an unusually high value for $Y_{\rm He}$. This is likely caused by the degeneracy between effective temperature and surface helium abundance at high temperatures (resulting from the loss of He I as a diagnostic). The large uncertainties in the determination of the micro-turbulent velocity show that this parameter cannot be constrained well with our data.

The errors on the parameters have been analyzed by calculating the probability ($P = 1 - \Gamma\left(\chi^2/2, \nu/2\right)$, where Γ is the incomplete gamma function and ν is the degrees of freedom) for all calculated models. Because P is very sensitive to the value of χ^2, we normalize all χ^2 values such that the best $\chi^2_{\rm red}$ is equal to 1, i.e., we assume that deviations of the original best $\chi^2_{\rm red}$ from unity are induced by under- or overestimated error bars on the normalized flux. This approach is similar in spirit to using relative weighting in the χ^2 merit function and to propagating the root mean square of the fit to scale the error bars (e.g., Press et al. 1986). The uncertainties are obtained by considering the range of models which satisfy $P > 5\%$. These errors do not take into account uncertainties in the luminosity. However, as the mass-loss rate approximately scales with luminosity as $\dot{M} \propto L^{5/4}$, typical uncertainties in L do not have a significant impact on our conclusions.

4. RESULTS AND DISCUSSION

The derived mass-loss rates are represented in the modified wind momentum versus luminosity diagram (WLD; Figure 3). The modified wind momentum is defined as $D_{\rm mom} = \dot{M} v_\infty \sqrt{R/R_\odot}$. This quantity is ideally suited to study the $\dot{M}(Z)$ relation because it is almost independent of mass, and v_∞ and R are usually relatively well constrained. As the Hα recombination line is essentially sensitive to the invariant wind-strength parameter $Q = \dot{M}/(R^{3/2} v_\infty)$ that is inferred from the spectral analysis, D (for given $T_{\rm eff}$) scales with L, making it less sensitive to uncertainties in the luminosity. As v_∞ is expected to scale with metallicity ($v_\infty \propto Z^{0.13}$; Leitherer et al. 1992), and the wind-strength parameter Q is invariant, the derived mass-loss rate is subject to a similar scaling. This scaling of $\dot{M}$ and v_∞ has been applied to the values given in Table 2.

Compared to theoretical expectations (Vink et al. 2001; $Z = 0.14\,Z_\odot$ dashed line in Figure 3), all stars except IC 1613-A13 tend toward a higher than predicted mass-loss rate for their metallicity. Compared to the empirical relations found by Mokiem et al. (2007), our values are reminiscent of the values measured for the LMC. For IC 1613-A15 we could only obtain an upper limit due to the nebular contamination, and IC 1613-B11 and C9 could have a low enough mass-loss rate within the errors. WLM-A11 and NGC 3109-20 have a well-defined mass-loss rate which is almost an order of magnitude too large for their metallicity.

4.1. Systematic Uncertainties in the Mass-loss Determination

In addition to random uncertainties, several sources of systematic uncertainties may affect our mass-loss determinations, for instance due to assumptions we have made. Here we discuss potential non-intrinsic causes for the high mass-loss rates that we derive.

The adopted values of the flow acceleration parameter β could contribute to the high values of $D_{\rm mom}$. To fit the line profile, the wind density versus velocity profile must be the same, causing a higher value of β to give a lower mass-loss

Table 2
Best-fit Parameters and Derived Properties of the Observed Stars

ID	$T_{\rm eff}$ (kK)	log$g$ (cm s^{-2})	log$\dot{M}$ ($M_\odot$ yr^{-1})	$Y_{\rm He}$	$v_{\rm tur}$ (km s^{-1})	$v_{\rm rot}\sin i$ (km s^{-1})	v_∞ (km s^{-1})	log$L$ ($L_\odot$)	R ($R_\odot$)
IC 1613									
–A13	$47.6^{+4.73}_{-4.95}$	$3.73^{+0.13}_{-0.22}$	$-6.26^{+0.45}_{-0.50}$	$0.32^{+0.04}_{-0.17}$	$4^{+25}_{\downarrow}$	94^{+40}_{-28}	1869	5.78	11.4
–A15	$33.7^{+3.10}_{-2.65}$	$3.76^{\uparrow}_{-0.39}$	$-6.36^{+0.40}_{\downarrow}$	$0.16^{+0.14}_{-0.10}$	$9^{+17}_{\downarrow}$	34^{+42}_{-24}	1971	5.24	12.2
–B11	$31.3^{+2.00}_{-2.00}$	$3.41^{+0.24}_{-0.21}$	$-6.16^{+0.30}_{-1.30}$	$0.13^{+0.11}_{-0.07}$	$12^{+13}_{\downarrow}$	88^{+36}_{-28}	1601	5.45	18.1
–C9	$35.7^{+1.70}_{-1.85}$	$3.58^{+0.19}_{-0.24}$	$-6.26^{+0.25}_{-0.60}$	$0.12^{+0.10}_{-0.04}$	$15^{+8}_{\downarrow}$	72^{+28}_{-28}	1697	5.43	13.6
WLM									
–A11	$29.7^{+2.45}_{-2.75}$	$3.25^{+0.29}_{-0.19}$	$-5.56^{+0.20}_{-0.30}$	$0.11^{0.11}_{\downarrow}$	$8^{+14}_{\downarrow}$	70^{+40}_{-36}	1711	5.79	29.8
NGC 3109									
–20	$34.2^{+4.70}_{-3.05}$	$3.48^{+0.37}_{-0.40}$	$-5.41^{+0.25}_{-0.35}$	$0.11^{\uparrow}_{\downarrow}$	$16^{\uparrow}_{\downarrow}$	98^{+86}_{-72}	2049	5.88	24.7

Note. Arrows indicate upper or lower limits.

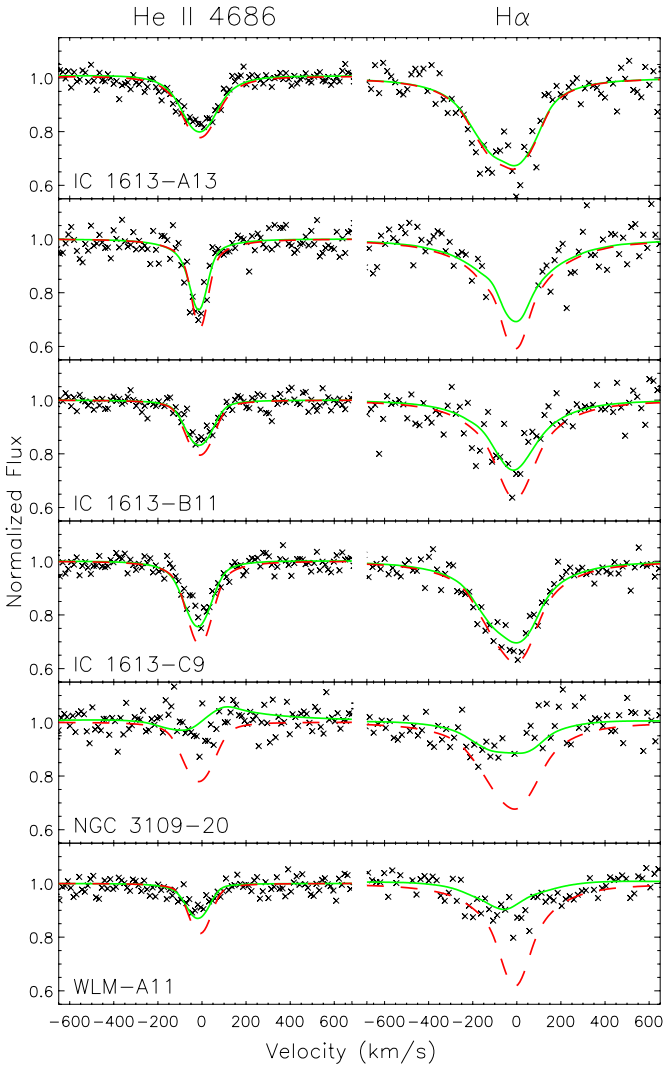

Figure 2. Line profiles of the mass-loss sensitive diagnostic lines He II 4686 and Hα. The best-fit line profiles are overplotted with solid lines. The dashed profiles indicate models with mass-loss rates predicted by radiation-driven wind theory.

(A color version of this figure is available in the online journal.)

rate. If we underestimated β the mass-loss rate will therefore be too high. However, even for extreme values of β, the correction will be at most a factor of two. The assumption

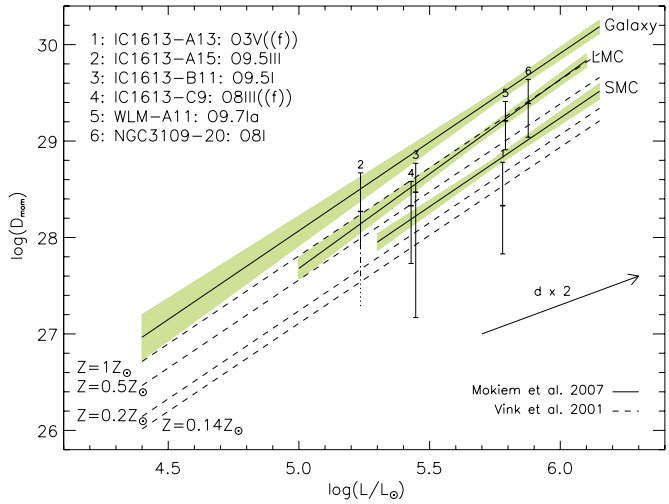

Figure 3. Modified wind momentum vs. luminosity diagram with our results. The dashed lines indicate the theoretical predictions of Vink et al. (2001), and the empirical results from Mokiem et al. (2007) are represented by the shaded bars. The arrow illustrates the effect of an uncertainty in the distance on the location of points in the diagram.

(A color version of this figure is available in the online journal.)

that $v_\infty = 2.6\ v_{\rm esc}$ introduces an uncertainty in $D_{\rm mom}$, but as errors in the terminal flow velocities are not expected to exceed 20%–40% (Groenewegen et al. 1989), this effect is even smaller.

Another source of uncertainty is the luminosity determination, both through extinction and distance uncertainties. However, as said before, the WLD is not very sensitive to uncertainties in L, as an increase in L almost linearly increases the value of $D_{\rm mom}$. This effect is illustrated by the arrow in Figure 3, indicating a change of a factor of two in distance. Furthermore, since the extinction toward all galaxies appears very low and the absolute magnitude of the stars (Table 1) agrees well with the values for their spectral type (Martins et al. 2005), we do not expect significant error in the luminosity.

An underestimated metallicity could also be part of an explanation for the difference in empirical and predicted mass-loss rates. However, the various studies mentioned in Section 2.2 all agree on an oxygen abundance of 10%–15% solar. Our own determination of the oxygen abundance for IC 1613 and NGC 3109 also agrees with these values. Furthermore, earlier studies on the stellar populations of our target galaxies (Cole et al. 1999; Minniti & Zijlstra 1997; Minniti et al. 1999) derived iron abundances of again 10%–15% solar.

Finally, multiplicity could play a role. Since the observed spectroscopic binary fraction in the Galaxy is approximately 50% (Mason et al. 2009; Sana & Evans 2010), it is possible that some of our sources are binaries. Binarity can influence the derived mass-loss rate by dilution or wind–wind collisions. In the case of a low-mass companion, the normalized spectrum will have shallower lines due to dilution effects. In close binaries with two massive stars, wind–wind collisions can cause emission in He II λ4686 and Hα if the wind-collision region is isothermal (see, for example, Sana et al. 2001). However, we could not find indications for massive companions in our data, which would cause higher luminosities, nor of radial velocities that differ from those of the parent galaxy.

Because of the large distance to the host galaxies, it is possible that our targets are unresolved multiples instead of single stars (e.g., O. Hartoog et al. 2012, in preparation). With a seeing of 0.″8, the smallest resolved area covers a distance ranging from 2.8 pc for IC 1613 to 5 pc for NGC 3109, and can therefore easily harbor a typical open cluster. However, the observed luminosities are typical of stars of the corresponding spectral type (Martins et al. 2005), and we therefore do not see any strong indications for multiplicity.

4.2. Possible Intrinsic Causes for the High Mass-loss Rates

There are several physical mechanisms that can increase the mass-loss rate or make it appear higher. A likely cause is the effect of wind clumping, which we do not take into account in our modeling. Clumping causes mass-loss indicators based on the average squared density $\langle\rho^2\rangle$, such as Hα, to have more emission than would be the case in an unclumped wind. This causes the derived mass-loss rates to be overestimated by a factor of $1/\sqrt{f}$, with f being the mean value of the volume-filling factor in the line-forming region (Puls et al. 2008).

However, by comparing our results to the relations found by Mokiem et al. (2007), where clumping is also unaccounted for (causing the empirical mass-loss rate to be higher than the theoretical prediction), the rates we find for $Z \sim 0.14\,Z_\odot$ galaxies coincide with LMC values. So unless clumping behaves differently at sub-SMC metallicities, we would still expect the mass-loss rates to be located below the empirical SMC area in the WLD.

The slope and absolute scaling of the WLD is also anticipated to change at very low metallicities (Kudritzki 2002). The expected effect, however, works in the opposite direction, and the mass-loss rates should be even lower. Furthermore, the slope change is predicted to occur at a much lower metallicity ($Z \approx 10^{-3}\,Z_\odot$).

Fast rotation can cause an increased and asymmetric mass loss (e.g., Maeder & Meynet 2000). However, all of the projected rotational velocities we derive are low ($v \sin i < 100$ km s^{-1}), and given that the probability that by chance all sources have their rotational axis pointed more or less in our direction is small, we do not expect this effect to play a major role in our sample.

There could be other processes affecting the mass-loss process, possibly related to pulsations and magnetic fields, which both have been detected in O-type stars (e.g., Henrichs 1999; Donati & Landstreet 2009). Pulsations are caused by the high sensitivity of opacity to temperature in the high-temperature low-density regions in O (super)giants, giving rise to κ-pulsations (e.g., Iglesias et al. 1992). This is induced by the sudden appearance of a large number of same-shell transition iron lines, and is therefore dependent on the iron abundance. Thus, it is expected that pulsations are less important at low metallicities (Baraffe et al. 2001).

The increased opacity described above can give rise to small convective regions in the stellar envelope (Cantiello et al. 2009). Cantiello & Braithwaite (2011) showed that these convective regions can produce magnetic hot spots through the dynamo effect, which can be strong enough to influence the wind and possibly play a role in the wind clumping. This effect is again metallicity dependent, and is expected to play a lesser role and eventually disappear with decreasing metallicity (Cantiello et al. 2009).

5. CONCLUSIONS AND IMPLICATIONS

In this Letter, we have pointed out a discrepancy between the observed and predicted mass-loss rates from massive stars in low-metallicity environments, and discussed possible explanations.

A potential violation of the expected metallicity scaling of the radiation-driven mass-loss rate at $Z \sim 1/7\,Z_\odot$, resulting in higher than expected mass-loss rates, would have far-reaching implications. First, one expects low-Z O-type stars to suffer more from spin-down through angular momentum loss in the stellar wind. Consequently, the rotational mixing efficiency may be reduced, leading, for instance, to a more modest nitrogen enrichment than currently thought (Brott et al. 2011).

Second, one anticipates the single O-star population in low-metallicity environments to produce more observationally identifiable Wolf–Rayet stars, being the successors of O-type stars having their outer envelope stripped by mass loss, and therefore increased number of Ib and, potentially, Ic supernovae. The single-star channel would, however, produce less progenitors of long-duration gamma-ray bursts, as the stars lose more angular momentum by their outflow.

Finally, if the larger than expected wind strength at $Z \sim 1/7\,Z_\odot$ persists to extremely low metallicities (though at present the driving mechanism is unknown), stellar winds will impact the evolution of massive Population III stars and the chemical enrichment of the intergalactic medium of the early universe.

We thank the referee, Dr. Kudritzki, for his useful comments, Dr. Martayan for his support during the observations, and O. Hartoog for the interesting discussions.

Facility: VLT:Kueyen (X-Shooter)

REFERENCES

Baraffe, I., Heger, A., & Woosley, S. E. 2001, ApJ, 550, 890
Bresolin, F., Gieren, W., Kudritzki, R.-P., et al. 2009, ApJ, 700, 309
Bresolin, F., Pietrzyński, G., Urbaneja, M. A., et al. 2006, ApJ, 648, 1007
Bresolin, F., Pietrzyński, G., Urbaneja, M. A., et al. 2007, ApJ, 671, 2028
Brott, I., de Mink, S. E., Cantiello, M., et al. 2011, A&A, 530, 115
Cantiello, M., & Braithwaite, J. 2011, A&A, in press (arXiv:1108.2030)
Cantiello, M., Langer, N., Brott, I., et al. 2009, A&A, 499, 279
Castor, J. I., Abbott, D. C., & Klein, R. I. 1975, ApJ, 195, 157
Charbonneau, P. 1995, ApJS, 101, 309
Cole, A. A., Tolstoy, E., Gallagher, J. S., et al. 1999, AJ, 118, 1657
Davidge, T. J. 1993, AJ, 105, 1392
D'Odorico, S., Dekker, H., Mazzeloni, R., et al. 2006, Proc. SPIE, 6269, 626933
Donati, J.-F., & Landstreet, J. D. 2009, ARA&A, 47, 333
Evans, C. J., Bresolin, F., Urbaneja, M. A., et al. 2007, ApJ, 659, 1198
Goldoni, P., Royer, F., François, P., et al. 2006, Proc. SPIE, 6269, 62692
Groenewegen, M. A. T., Lamers, H. J. G. L. M., & Pauldrach, A. W. A. 1989, A&A, 221, 78
Heger, A., Jeannin, L., Langer, N., & Baraffe, I. 1997, A&A, 327, 224
Henrichs, H. F. 1999, in IAU Conf. 169, Variable and Non-spherical Stellar Winds in Luminous Hot Stars, ed. B. Wolf et al. (Lecture Notes in Physics, Vol. 523; Berlin: Springer-Verlag), 304

Herrero, A., Garcia, M., Uytterhoeven, K., et al. 2011, in IAU Symp. 272, Active OB Stars: Structure, Evolution, Mass-Loss, and Critical Limits, ed. C. Neiner et al. (Cambridge: Cambridge Univ. Press), 292
Humphreys, R. M., & Davidson, K. 1994, PASP, 106, 1025
Iglesias, C. A., Rogers, F. J., & Wilson, B. G. 1992, ApJ, 397, 717
Kudritzki, R. P. 2002, ApJ, 577, 389
Kudritzki, R., & Puls, J. 2000, ARA&A, 38, 613
Lamers, H. J. G. L. M., Snow, T. P., & Lindholm, D. M. 1995, ApJ, 455, 269
Leitherer, C., Robert, C., & Drissen, L. 1992, ApJ, 401, 596
Maeder, A., & Meynet, G. 2000, A&A, 361, 159
Martins, F., Schaerer, D., & Hillier, D. J. 2005, A&A, 436, 1049
Mason, B. D., Hartkopf, W. I., Gies, D. R., Henry, T. J., & Helsen, J. W. 2009, AJ, 137, 3358
Minniti, D., & Zijlstra, A. A. 1997, AJ, 114, 147
Minniti, D., Zijlstra, A. A., & Alonso, M. V. 1999, AJ, 117, 881
Modigliani, A., Goldoni, P., Royer, F., et al. 2010, Proc. SPIE, 7737, 773728
Mokiem, M. R., de Koter, A., Puls, J., et al. 2005, A&A, 441, 711
Mokiem, M. R., de Koter, A., Vink, J. S., et al. 2007, A&A, 473, 603
Mokiem, M. R., Martín-Hernández, N. L., Lenorzer, A., de Koter, A., & Tielens, A. G. G. M. 2004, A&A, 419, 319
Pagel, B. E. J., Edmunds, M. G., Blackwell, D. E., Chun, M. S., & Smith, G. 1979, MNRAS, 189, 95
Pietrzyński, G., Gieren, W., Soszyński, I., et al. 2006, ApJ, 642, 216
Pilyugin, L. S., & Thuan, R. X. 2005, ApJ, 631, 231
Press, W. H., Flannery, B. P., Teukolsky, S. A., et al. 1986, Numerical Recipes: The Art of Scientific Computing (Cambridge: Cambridge Univ. Press)
Puls, J., Urbaneja, M. A., Venero, R., et al. 2005, A&A, 435, 669
Puls, J., Vink, J. S., & Najarra, F. 2008, A&ARv, 16, 209
Sana, H., & Evans, C. J. 2010, in IAU Symp. 272, Active OB Stars: Structure, Evolution, Mass-Loss, and Critical Limits, ed. C. Neiner et al. (Cambridge: Cambridge Univ. Press), 474
Sana, H., Rauw, G., & Gosset, E. 2001, A&A, 370, 121
Schlegel, D. J., Finkbeiner, D. P., & Davis, M. 1998, ApJ, 500, 525
Smith, N., Vink, J. S., & de Koter, A. 2004, ApJ, 615, 475
Soszyński, I., Gieren, W., Pietrzyński, G., et al. 2006, ApJ, 648, 375
Urbaneja, M. A., Kudritzki, R.-P., Bresolin, F., et al. 2008, ApJ, 684, 118
Vernet, J., Dekker, H., d'Odorico, S., et al. 2011, A&A, in press
Vink, J. S., de Koter, A., & Lamers, H. J. G. L. M. 2001, A&A, 369, 574
Woosley, S. E., & Bloom, J. S. 2006, ARA&A, 44, 507
Yoon, S.-C., & Cantiello, M. 2010, ApJ, 717, L62
Yoon, S.-C., & Langer, N. 2005, A&A, 433, 643